

Document downloaded from:

<http://hdl.handle.net/10251/28622>

This paper must be cited as:

Aznar Gimeno, E.; Sancenón Galarza, F.; Marcos Martínez, MD.; Martínez Mañez, R.; Amoros Del Toro, P.; Cano, J.; Stroeve, P. (2012). Delivery modulation in silica mesoporous supports via alkyl chain pore outlet decoration. *Langmuir*. 28:2986-2996.
doi:10.1021/la204438j.



The final publication is available at

<http://pubs.acs.org/doi/ipdf/10.1021/la204438j>

Copyright American Chemical Society

Additional Information

Delivery modulation in silica mesoporous supports via alkyl chain pore outlet decoration.

Elena Aznar,^{§,†} Félix Sancenón,^{†,‡,§} M. Dolores Marcos,^{†,‡,§} Ramón Martínez-Máñez,^{†,‡,§} Pieter Stroeve,[⊥] Joan Cano^{||} and Pedro Amorós.[#]

[†]Centro de Reconocimiento Molecular y Desarrollo Tecnológico (IDM). Unidad Mixta Universitat Politècnica de València-Universitat de València, Spain.

[‡]Departamento de Química. Universitat Politècnica de València. Camino de Vera s/n, 46022, Valencia, Spain.

[§]CIBER de Bioingeniería, Biomateriales y Nanomedicina (CIBER-BBN).

[⊥]Department of Chemical Engineering and Materials Science, University of California Davis, Davis, California 95616, United States.

^{||}Instituto de Ciencia Molecular (ICMol) and Fundació General de la Universitat de València (FGUV), Universitat de València, Paterna, Valencia, E-46980 Spain.

[#]Institut de Ciència dels Materials (ICMUV), Universitat de València, P.O. Box 22085, E-46071, Valencia, Spain.

E-mail: rmaez@qim.upv.es, pstroeve@ucdavis.edu

RECEIVED DATE (to be automatically inserted after your manuscript is accepted if required according to the journal that you are submitting your paper to)

CORRESPONDING AUTHOR: Prof. Ramón Martínez-Máñez. Fax: (+34) 96-387-93-49. E-mail: rmaez@qim.upv.es. Prof. Pieter Stroeve. Fax (530) 752-1031. E-mail: pstroeve@ucdavis.edu

ABSTRACT

This paper focuses on the study of the release rate in a family of modified silica mesoporous supports. A collection of solids containing ethyl, butyl, hexyl, octyl, decyl, octadecyl, docosyl and triacontyl groups anchored on the pore outlets of mesoporous MCM-41 has been prepared and characterized. Controlled release from pore voids has been studied through the delivery of the dye complex tris(2,2'-bipyridyl)ruthenium(II). Delivery rates were found to be dependent on the alkyl chain length anchored on the pore outlets of the mesoporous scaffolding. Moreover, release rates follow a Higuchi diffusion model and Higuchi constants for the different hybrid solids have been calculated. A decrease of the Higuchi constants was observed as the alkyl chain used to tune the release profile is longer confirming the effect that the different alkyl chains anchored into the pore mouths exerted on the delivery of the cargo. Furthermore, in order to better understand the relation between pore outlets decoration and release rate, studies using molecular dynamics simulations employing force-field methods have been carried out. A good agreement between the calculations and the experimental observations was observed.

KEYWORDS: Controlled release, mesoporous supports, diffusion, alkyl chains.

INTRODUCTION

Since the 20th century second half, chemical species controlled release had been a very active research field. The delivery of certain compounds or drugs in a controlled fashion is of crucial interest in many scientific disciplines such as biology, pharmacology and medicine. For this reason a great amount of new delivery dispositives using several strategies have been developed. For instance, microcapsules,¹ micelles,² vesicles,³ dendrimers⁴ or polymeric matrixes⁵ have been extensively used for controlled

release of target guests. Silica mesoporous supports (SMPS), discovered at the end of the past century, made researchers to focus their attention in a new approach for cargo storage and delivery. The reasons of interest were mainly related to the distinctive characteristics of SMPS such as their high surface area, inertness, thermal stability, the presence of tunable pore sizes with a diameter of ca. 2-10 nm, homogeneous pore distribution and the well-known procedures that can be used for their surface functionalization.⁶ The first silica mesoporous-based system for controlled release of chemical species was prepared by the Vallet-Regí research group. In this pioneering work a MCM-41 scaffold was loaded with ibuprofen as a model compound and the drug delivery kinetics was studied. The authors showed that it was possible to design drug release systems selecting the appropriate matrix and cargo.⁷ Later, the same authors reported that inner silica surface functionalization with certain organic moieties, which could give supramolecular interactions with the guest, is an ideal way to accommodate the molecules and also to control the delivery rate.⁸ This simple load and delivery methodology using SMPS has been extensively used, but in some cases presents certain limitations such as the possible irreversible lost of functionality, and the difficulty in the design of systems capable of both molecule accommodation and appropriate sustained release.

In a further advance in this field, the possibility of incorporating in the external surface of SMPS functional groups capable of being opened or closed at will has resulted in the design of gated hybrid mesoporous supports for advanced control delivery applications. In fact, the unique architecture of SMPS containing parallel pores with two unique openings, makes it possible to design gated systems able to achieve zero release and which can be fully opened on-command using a variety of physical, chemical or biochemical stimuli.⁹ For instance, gated SMPS displaying controlled release features using light, redox reactions, pH changes and biomolecules have been described.

The first gate-like hybrid material was developed by Fujiwara et al.¹⁰ Their innovative system was able to control cholestane and other molecules transport by irradiation with the appropriate light due to the reversible photodimerization of coumarin molecules that were decorating the pore outlets. Since then, some light-triggered systems based on *cis-trans* isomerization of azobenzene moieties,¹¹

supramolecular interactions between α -cyclodextrin and photosensitive azobenzene groups,¹² or photoswitchable molecules as spiropyrans¹³ have been reported. Another widely used stimulus is pH. Since some of us reported in 2004 the first gated hybrid support operative in an aqueous solution, using SMPS functionalized with polyamines on the external surface that can be tuned under pH and anion control,¹⁴ additional systems involving carboxylates¹⁵ pseudorotaxanes,¹⁶ inclusion complexes with cucurbit[6]uril,¹⁷ cucurbit[7]uril,¹⁸ and α -cyclodextrins¹⁹ have been also described. Furthermore a combination of pH and other stimuli has been achieved highlighting the importance of that operational mode.²⁰ Redox-driven gate-like scaffoldings are up to the same standard that pH. Lin's pioneering group has developed hybrid solids using mesoporous scaffoldings capped with CdS, gold, or magnetic nanoparticles attached through disulfide linkages that were broken up upon addition of certain reducing compounds.²¹ Using this kind of stimulus, Zink and Stoddart also prepared several gated materials based on redox-active rotaxanes and pseudorotaxanes moieties.²² Apart from the examples that use redox-,²³ light-, and pH-triggered²⁴ systems, some alternative stimuli have been used such as temperature²⁵ or the presence of certain small molecules.²⁶ Moreover, in the last years, gated SMPS able to deliver the cargo triggered by bio-molecules have attracted the attention of researchers and for instance enzyme-activated systems,²⁷ hybrid functional materials using antigen-antibody interactions,²⁸ aptamer-target recognition²⁹ or oligonucleotide hybridization³⁰ have been used in mesoporous supports for controlled release applications.

The above are nice examples that show the appearance of synergistic features arising from the combination of solid structures and suitable functional groups which results in the development of new and more sophisticated systems showing enhanced delivery properties.³¹ In these systems surface functionalisation is a key issue. In relation to this surface chemical modification, apart of the gated ensemble that control the opening or close of the pores, it is also possible to built molecular obstacles at the pore outlets able to modulate mass transport at the nanometric level. Moreover, this operational way that could achieve tuned release via barrier formation at the pore mouths, will not be an impediment for the possible chemical modification of the inner pore surface with the objective of guest loading in the

pore voids. Following this approach the design of more complex delivery systems in which the events of guest accommodation (via functionalisation of the inner pores), on-command delivery (via anchoring capped or gated ensembles) and modulation of the delivery rate (via incorporation of molecular obstacle at the pore outlets) can be envisioned.

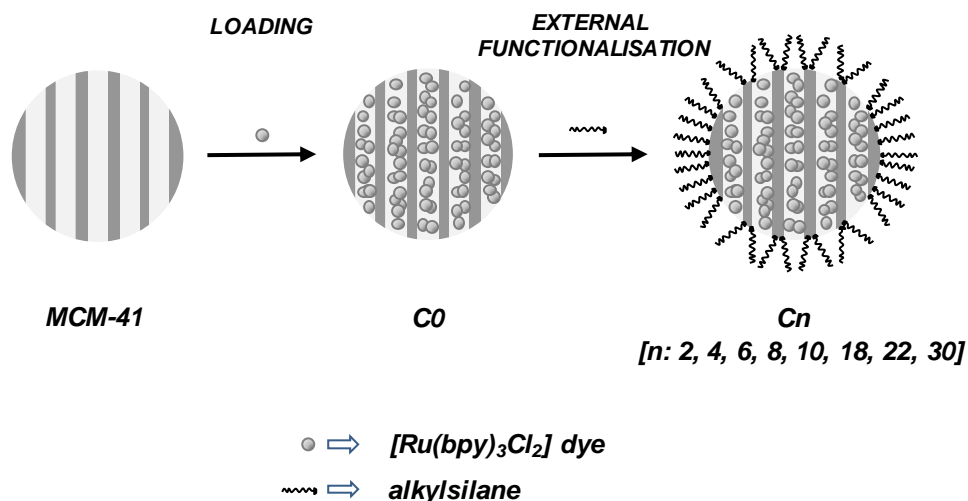
In this present work we have focused our attention to the control in the delivery rate via the chemical modification of the pore entrances on SMPS by covalent bonding of aliphatic chains as model barriers. It was expected that different length chains could lead a change in guest delivery rate from the inner pores to the solution, allowing a tuned release of the cargo. This effect has been studied through the delivery of a model compound (a ruthenium(II) dye probe) and it is discussed in terms of the release time and the Higuchi diffusion model. Moreover, in order to better understand the relation between the pore outlets decoration and delivery, the results have been studied according to molecular dynamics simulations using force-field methods.

RESULTS AND DISCUSSION

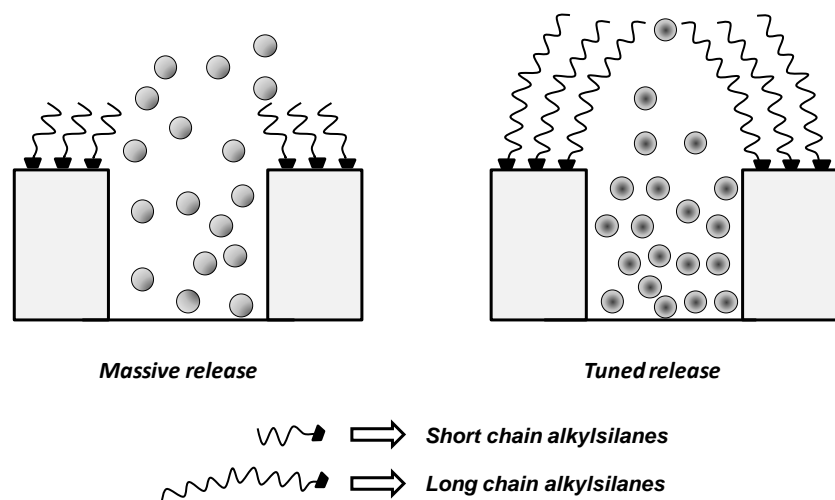
Design and synthesis. For the design of hybrid materials for tuned release, we selected a nanoparticulated mesoporous material of the MCM-41 family as a suitable inorganic support, due to its high homogeneous porosity, inertness and ease of functionalization on its surface. As diffusion controllers (molecular obstacles at the pore outlets), we used alkyl chains of different length that were anchored on the external surface of the mesoporous material. For monitoring purposes, we selected the dye tris(2,2'-bipyridyl)ruthenium(II) chloride as probe that has been widely used to study the functional open/close protocol in gated materials depicted in Scheme 2.

To ensure the right arrangement of the constituent building blocks, these should be set out in a programmed mode. Thus, the silica mesoporous nanoparticles must contain the cargo in the pores, whereas the alkyl chains should ideally only be anchored in the pore outlets. In order to achieve this organization we first prepared the support and suspended it in a solution of the tris(2,2'-bipyridyl)ruthenium(II) chloride in acetonitrile. Then, after removal of adsorbed water in the solid by

distillation, the suspension was stirred for 24 hours at room temperature with the aim of completely loading the pores of the MCM-41 scaffolding. The final orange solid (C0) was filtered, washed with acetonitrile and dried at 50 °C for 12 hours. To obtain solids C_n, where **n** is the number of carbons of the alkyl chain, C0 solid was suspended in anhydrous toluene, in which ruthenium (II) complex is insoluble, and the corresponding organosilane was added to the suspension under vigorous stirring. The resulting orange solid was filtered, washed with toluene and dried at 50 °C for 12 h. This synthetic procedure assures a preferential grafting of the alkyl chains in the external surface rather than inside the pore walls, which are filled by the ruthenium (II) dye. Following this synthetic protocol (see the Experimental Section for further details) a collection of hybrid solids containing chains of 2, 4, 6, 8, 10, 18, 22 and 30 carbon atoms appended on the pore outlets have been prepared. Scheme 1 shows a schematic representation of the prepared solids functionalized with alkyl chain length grafted in the mesopore mouths.



Scheme 1. Representation of the synthetic procedure to obtain hybrid solids



Scheme 2. Representation of alkyl chains tuning effect on guest release rate from mesopore voids to a solution.

Characterization of functional hybrid solids. All new solids were characterized using standard procedures. Figure 1 shows powder X-ray diffraction patterns of the nanoparticulated MCM-41 support, the **C0** solid and the **C22** functionalized material. Powder XRD of siliceous nanoparticulated MCM-41 as-synthesized (curve a) shows four low-angle reflections typical of a hexagonal array that can be indexed as (100), (110), (200) and (210) Bragg peaks. A displacement of the (100) peak in the powder XRD of the nanoparticulated MCM-41 calcined sample is clearly appreciated in curve b, corresponding to an approximate cell contraction of 7 Å. This displacement and the broadening of the (110) and (200) peaks are related to further condensation of silanol groups during the calcination step. Curve c corresponds to the **C0** powder XRD pattern. In this case, a slight intensity decrease of the (100) reflection and a broadening of the (110) and (200) reflections is observed, most likely related to a loss of contrast due to the filling of the pore voids with the ruthenium (II) dye. Finally, curve d corresponds to the **C22** powder XRD pattern in which the typical peak (100) is still observed confirming that the structure is not affected after the loading of the dye and the covalent bonding of the corresponding alkyl chain at the pore outlets. Powder XRD of all the remaining hybrid solids are similar to that of solid **C22**. Furthermore, these results are consistent with TEM studies. Inset of Figure 1 shows a representative image of solid **C22** (similar images were found for the other hybrid solids) where the typical hexagonal

porosity of MCM-41 matrix can be observed. In addition, the image also evidences the spherical morphology of the particles with a diameter around 100-200 nm.

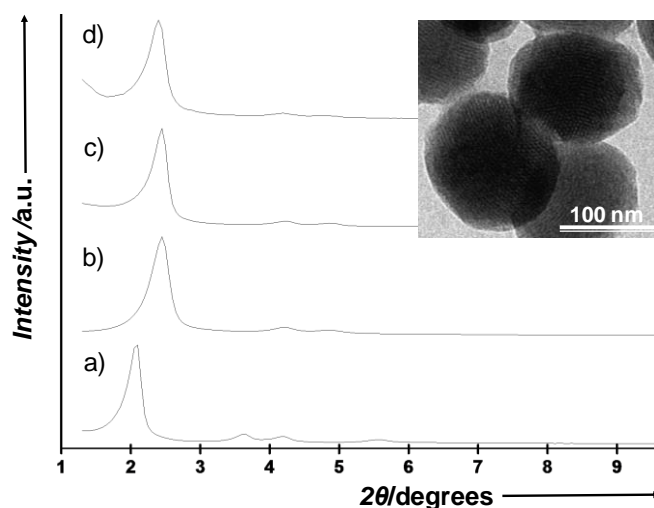


Figure 1. Powder X-ray diffraction patterns of the solids (a) MCM-41 as-synthesized (b) calcined MCM-41 (c) solid **C0** containing the ruthenium (II) dye and (d) solid **C22** containing the ruthenium dye and docosyl chains at the pore outlets (similar for the rest of **C_n** solids). Inset: Representative TEM image of **C22**.

Isothermal N₂ adsorption-desorption studies of the nanoparticulated MCM-41 calcined material, the dye-loaded material **C0** and selected **C4** and **C18** hybrid solids were carried out. MCM-41 scaffolding curves show two sharp adsorption steps (see Figure 2, black filled points). The isotherm of this parent silica shows a first step at intermediate P/P_0 values (0.1-0.4) typical of mesoporous solids related to the nitrogen condensation inside the mesopores by capillarity. The absence of a hysteresis loop in this interval and the narrow pore distribution suggest the existence of uniform cylindrical mesopores with a pore volume of 0.68 cm³ g⁻¹ calculated by using the Barret, Joyner and Halenda (BJH) model on the adsorption branch of the isotherm. The application of the Brunauer-Emmett-Teller (BET) model resulted in a value for the total specific surface of 870.6 m²/g. From the powder XRD, porosimetry and TEM studies, the a_0 cell parameter (4.16 nm), the pore diameter (2.44 nm) and a value for the wall thickness (1.72 nm) were calculated. In addition to this adsorption step associated to the micelle generated mesopores, a second feature appears in the isotherm at a high relative pressure ($P/P_0 > 0.8$). This second

step corresponds to the filling of the large voids among the particles that must be considered as a textural-like porosity ($0.25 \text{ cm}^3/\text{g}$). In this case, curves show a characteristic H1 hysteresis loop and a wide pore size distribution.

The N_2 adsorption-desorption isotherms of samples **C0**, **C4** and **C18** that are shown in Figure 2 (white filled points) are typical of mesoporous materials with partially filled pores. BET specific surface values, and BJH pore volumes and sizes, calculated from the N_2 adsorption-desorption isotherms are listed in Table 1. In all samples the dye uptake (in **C0**, **C4** and **C18**) and the functional groups grafting (in **C4** and **C18**) leads to a significant decrease in the pore volume and surface area when compared to the parent silica. The most relevant feature is the absence of a sharp step at low-medium relative pressure ($0.1 < P/P_0 < 0.4$). In fact, although the two typical adsorption steps clearly remain, these solids shows a remarkable decrease of nitrogen absorption in that region when compared (at the same scale) to those of the MCM-41 calcined support, which suggests that pore voids are filled in a large extent with the dye or blocked with the alkyl chains. Moreover, a regular tendency with the alkyl chain length is observed. Then, for similar values of dye uptake (see below), a more efficient blocking effect is observed as the alkyl chain length increases when compared with the absence of hydrocarbonated groups (**C0**). Hence, BET surface area decrease of a 49.5%, 60.5% and 68.9% is observed for samples **C0**, **C4** and **C18**, respectively (when compared to MCM-41). In a similar way, the intra-particle mesopore volume ($P/P_0 < 0.6$) also decreases a 50.9%, 67.6% and 72.1% for samples **C0**, **C4** and **C18**, respectively. This tendency of the intra-particle porosity does not affect in a significant way to the mesoporous size. Although wider BJH mesopore size distributions can be appreciated for samples **C0**, **C4** and **C18** when compared to MCM-41, it must be remarked that the maximum in their respective BJH distributions (see Table 1) clearly shifts towards lower mesopore sizes: from 2.44 nm (MCM-41) to values in the 2.24-2.34 nm range. Assuming that the dye loading process and the anchoring of the alkyl chains do not alter the silica walls, the remaining porosity for **C0**, **C4** and **C18** must be due to a certain proportion of empty or partially filled mesopores, since a certain dye leaching during the subsequent anchoring with alkyl groups cannot be completely discarded.

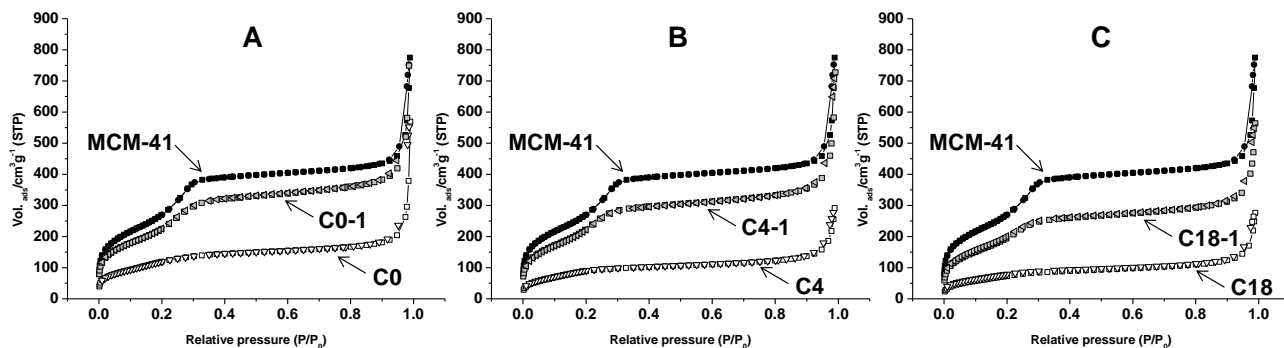


Figure 2. Nitrogen adsorption-desorption isotherms for MCM-41 mesoporous material, **C0** (A), **C4** (B) and **C18** (C) hybrid materials, and their corresponding dye released material (**C0-1**, **C4-1**, and **C18-1**).

Additionally, the curves show a N_2 adsorption at high relative pressure similar to the calcined MCM-41, confirming the presence of the textural porosity. Variations in the inter-particle textural pore volume and pore size observed can be associated to the synthetic procedure followed to obtain the hybrid solids, which implies solvent changes, even to a certain interparticle spacer-effect provided by alkyl groups hindering the usual aggregation of silica nanoparticles (in **C4** and **C18**). In any case, this large pore system has a low significance for the application described in this work.

In order to complete this study, delivery of the dye from solids **C0**, **C4** and **C18** was allowed in water for a long period of time and the resulting materials (**C0-1**, **C4-1** and **C18-1**) were characterized through N_2 adsorption-desorption isotherm studies (see Figure 2 and Table 2). These later solids show typical features of cylindrical empty mesopores with a sharp adsorption step at $0.1 < P/P_0 < 0.4$. Moreover, an increase in the nitrogen adsorption and BJH pore volume with respect to **C0**, **C4** and **C18** is observed after dye delivery. This partially recovered mesoporosity confirms that the dye was accommodated inside the mesopores of **C0**, **C4** and **C8** loaded materials.

From the obtained data, pore volume in the low-medium relative pressures can give some information of the role played by the alkyl chains decorating pore outlets of final hybrid materials. As it can be observed in Table 1, the mesopore volume of the unloaded materials ($P/P_0 < 0.6$) is recovered after dye release. In fact, the final achieved volume for samples **C0-1** (without chain), **C4-1** and **C18-1** is an

89.7%, 83.8% and 73.5% of the respective value for the parent silica. This similar evolution can be appreciated for the BET surface area values. Moreover, the fact that the porosity was not completely restored is probably due to the presence of a certain proportion of undelivered dye, that could be physisorbed in the pore walls (in **C0**, **C4** and **C18**) or even trapped or blocked by the alkyl chains anchored at the mesopore mouths (in **C4** and **C18**). This role played by the functional organic groups is supported by the BJH mesopore volumes evolution since the recovered mesoporosity (respect to the parent silica) decreases as the alkyl chain length increases.

Table 1. BET specific surface values, pore volumes and pore sizes calculated from the N₂ adsorption-desorption isotherms for selected materials.

	S_{BET} (m ² g ⁻¹)	BJH pore ($P/P_0 < 0.6$) ^a (nm)	Maximum at the BJH pore size distribution (nm)	BJH pore ($P/P_0 > 0.6$) ^b (nm)	Total pore volume ^c (cm ³ g ⁻¹)	Pore volume ($P/P_0 < 0.6$) ^d (cm ³ g ⁻¹)	Pore volume ($P/P_0 > 0.6$) ^e (cm ³ g ⁻¹)
MCM-41	870.6	2.44	2.44	30.65	0.93	0.68	0.25
C0	439.7	2.58	2.24	62.17	0.97	0.30	0.67
C0-1	810.3	2.44	2.44	42.26	1.29	0.61	0.68
C4	343.7	2.59	2.25	36.50	0.52	0.22	0.30
C4-1	824.9	2.36	2.25	46.79	1.25	0.57	0.68
C18	270.3	2.57	2.34	34.74	0.49	0.19	0.30
C18-1	720.7	2.37	2.37	36.86	0.98	0.50	0.48

^a Pore size estimated by using the BJH model applied on the adsorption branch of the isotherm, for $P/P_0 < 0.6$, which can be associated to the surfactant generated mesopores.

^b Pore size estimated by using the BJH model applied on the adsorption branch of the isotherm, for $P/P_0 > 0.6$, which can be associated to the textural porosity.

^c Total pore volume according to the BJH model.

^d Pore volume for $P/P_0 < 0.6$, which can be associated to the surfactant generated mesopores.

^e Pore volume for $P/P_0 > 0.6$, which can be associated to the textural porosity.

Moreover, the dry conditions achieved during the sample evacuation prior to the analysis probably favours a certain collapse of the hydrocarbon groups anchored to the pore entrances. In any case, the porosity data suggest that despite long alkyl chains do not prevent dye release (vide infra), they can exert

the desired effect on the matter traffic, changing the release rate of encapsulated molecules from the pore voids to the solution.

The quantification of the content of the alkyl chain and the ruthenium (II) complex for each solid was accomplished by thermogravimetric studies and elemental analysis. The results are summarized in Table 2. Typical dye content is in the 0.44-0.54 mmol/gSiO₂ range, whereas the anchored alkylic groups are in the 0.89-1.09 mmol/gSiO₂ range.

Table 2. Organic content and calculated $t_{1/2}$ and K_H for each prepared hybrid solid.

Solid	C atoms	Alkyl chain content (mmol g ⁻¹ SiO ₂)	Dye content (mmol g ⁻¹ SiO ₂)	$t_{1/2}$ [a] (s)	k_H [b]
C0	0	0	0.46	-	-
C2	2	0.89	0.44	-	-
C4	4	0.89	0.46	-	-
C6	6	0.92	0.44	-	-
C8	8	1.09	0.46	23	10.25
C10	10	0.91	0.54	39	8.32
C18	18	0.84	0.54	49	7.70
C22	22	0.96	0.51	72	5.52
C30	30	1.01	0.51	223	4.02

[a] Calculated time to deliver 50% of ruthenium(II) probe from pore voids

[b] Calculated Higuchi constant

The high content of alkyl groups anchored on the silica indicates that the functionalization is not restricted only to the external surface, and then a certain modification of the internal, but close to pore mouths, surface occurs. The ability of the alkyl-silanes to modify the internal surface even in the case of materials with filled mesopores (with guest species) has been previously documented.³² Taking into account that normal density of silanol groups in silica materials is 6 Si-OH nm⁻² and that the molecules used to modify the surface have three reactive groups (ethoxy-, methoxy- or chlorosilanes), the

maximum density of alkyl chains in the synthesized hybrid solids can be estimated around 2-3 molecules per nm^2 . As the average determined amount of alkyl chains is 0.99 mmol/gSiO_2 , it can be calculated a necessary surface of around 199 nm^2 to anchor all the alkyl chains in the case of 3 molecules/ nm^2 . On the other hand, an external surface area of the starting MCM-41 particles of $70 \text{ m}^2/\text{g}$ was determined from adsorption isotherms on the as-synthesized material. Then, it is calculated that around 129 nm^2 of the total internal surface will be modified with alkyl chain. Furthermore, from TEM images, we estimated that nanoparticles diameter was 100 nm . Thus, the average mesopore length would also be 100 nm . Bearing in mind that each mesopore has two entrances, we can estimate an effective functionalization of the mesopore of *ca.* 8 nm deep.

Moreover, with the aim to explore the possibility that longer alkyl chains could form a crystalline phase able to affect to the pore blockage, we have registered the infrared spectra of all the synthesized solids. Using this technique, the evaluation of the packing state of alkyl chains can be conducted through CH_2 asymmetric vibration.³³ Thus, alkyl chains crystalline state can be identified when the band appears below 2920 cm^{-1} . In our study, as it can be seen in Figure 3, the position of the mentioned band for solid **C30** is centered at 2919.7 cm^{-1} , suggesting that the long alkyl chains used do not form a crystalline phase. This behavior has also been observed for all the prepared solids.

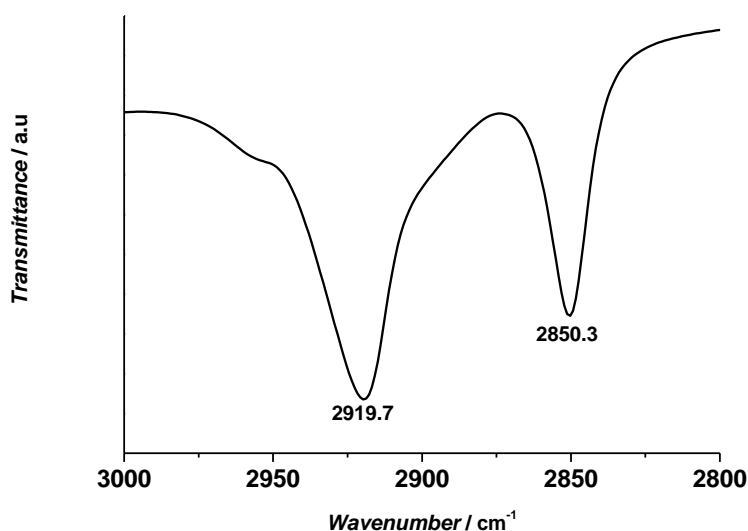


Figure 3.- Infrared spectra of solid **C30** showing the non crystallinity of the alkyl chains.

Controlled release. Controlled release performance of synthesized solids was straightforwardly studied via the delivery of the dye from the pore voids to the aqueous solution through monitorization of the visible band of the tris(2,2'-bipyridyl)ruthenium(II) chloride dye at 454 nm in the water phase. In a typical dye-release experiment, 2 mg of the corresponding solid and 10 mL of deionized water were maintained under constant vigorous stirring for a certain time and then, the suspension was filtered off through a 0.45 μ m nylon filter. The recorded absorption at 454 nm of the aqueous solution indicated the corresponding leak of dye from the pores. All the solids showed a quite rapid delivery rate since in all cases the maximum dye delivery was observed in less than two hours.

Figure 4 plots the dye release profiles for the different solids. The studies show that there is a very fast and similar release rate for solids **C0**, **C2**, **C4** and **C6**, indicating that when the pore outlets are decorated with short alkyl chains (0, 2, 4 and 6 carbon atoms, respectively), the organic modification of the pore mouth has a very low effect in dye payload. In contrast, solids **C8**, **C10**, **C18**, **C22** and **C30** having alkyl chains containing 8, 10, 18, 22 and 30 carbon atoms, respectively, show slower delivery rates, behavior that can be associated with the impediment exerted by the corresponding alkyl chain attached in the external surface. By a simple visual inspection it is evident that the longer the alkylic chain attached on the surface of the mesoporous solid the lower the delivery rate.

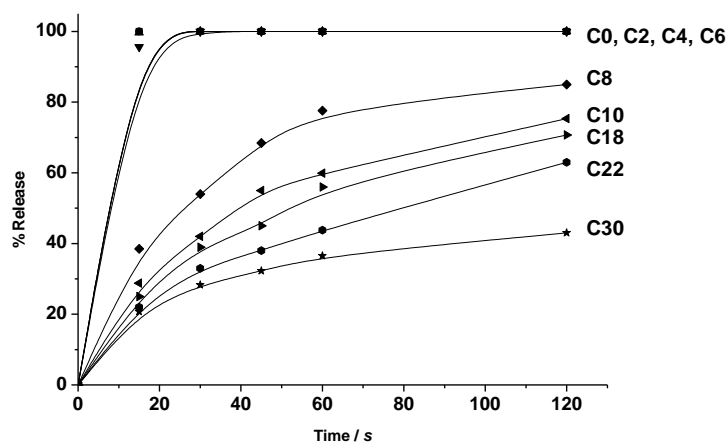


Figure 4.- Dye release profiles from pore voids of hybrid solids in the 0 to 120 seconds interval.

From obtained data for **C8**, **C10**, **C18**, **C22** and **C30** solids, the delivery profile can be adjusted to a logarithmic curve with the form $y = a \ln(x) + b$. Hence, the time necessary for delivery 50% of the dye ($t_{1/2}$) from solids **C8**, **C10**, **C18**, **C22** and **C30** was calculated and this value is shown in Table 2. The representation of calculated $t_{1/2}$ versus the number of carbon atoms of the alkyl chain (Figure 5) clearly shows an exponential trendline.

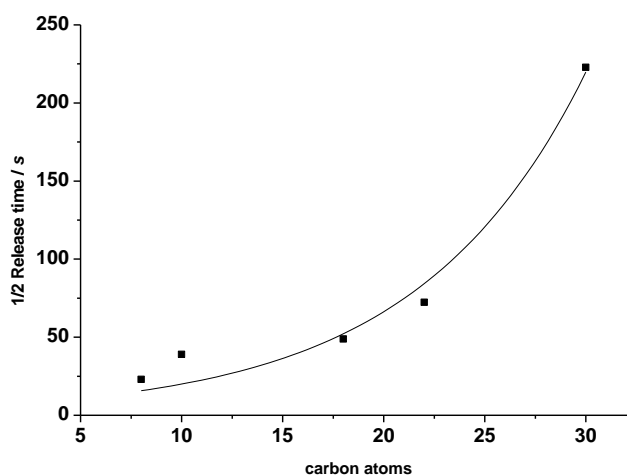


Figure 5.- Calculated $\frac{1}{2}$ release time versus the number of carbon atoms of the alkyl chain attached to the pore outlets for solids **C8**, **C10**, **C18**, **C22** and **C30**.

Moreover, differences observed in the ruthenium complex release rate from solids **C8**, **C10**, **C18**, **C22** and **C30** can be discussed in terms of a simple diffusion process from pore voids to the aqueous solution using the Higuchi model.³⁴ According to this model, release of species from pore voids is dependent on the square root of time when delivery is based on a Fickian diffusion process. Thus, the amount of guest release, Q_t , per unit of exposed area at time t can be described by the simple equation

$$Q_t = k_H \sqrt{t} \quad (1)$$

where k_H is the release rate constant for the Higuchi model. The k_H constant has been reported to depend basically on the diffusivity of the dye in the solvent, the porosity of the support, the tortuosity factor of the system, the amount of dye present in the matrix and its solubility in the solvent used, among other factors. With the aim to better understand the mass transport through porous systems,

Higuchi equation has been successfully applied the delivery profile shown in Figure 5 for solids **C8**, **C10**, **C18**, **C22** and **C30**.^{7,8} Figure 6 shows the graphical representation of the dye release from the pore voids to the solution versus the square root of time for solids **C8**, **C10**, **C18**, **C22** and **C30** and the lineal behavior observed.

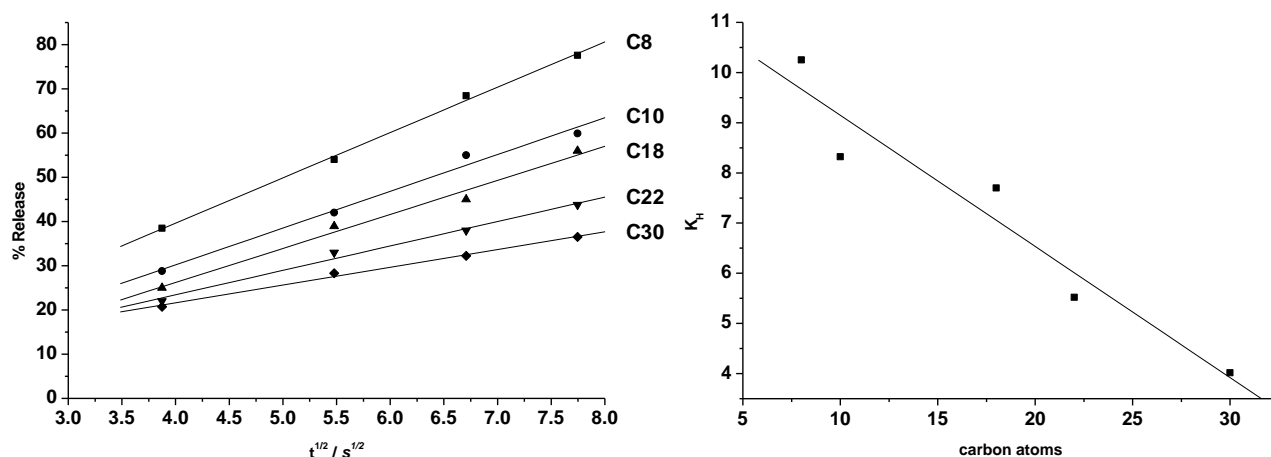


Figure 6.- Left; linear relationship of release versus the square root of the time for the delivery of the ruthenium (II) complex from the pores of solids **C8**, **C10**, **C18**, **C22** and **C30**. Right; release rate constant of the Higuchi model (k_H) versus the number of carbon atoms of the alkyl chain on solids **C8**, **C10**, **C18**, **C22** and **C30**.

The good linear fitting is indicative that the delivery of the dye from the pores of solids is basically a diffusive process. The calculated values of k_H are shown in Table 2. The plot of the calculated k_H constants versus the number of carbon atoms of the alkyl chains (Figure 6) shows that Higuchi constant decreases as the alkyl chain used to tune the release profile is longer.

Dynamic simulations. As we have seen above, the dye release rate from the pore voids in solids **Cn** is dependent of the length of the alkyl chain attached on the pore outlets of the mesoporous nanoparticles. In order to study this effect in further detail, the gated ensemble was studied by molecular dynamics simulations via force field methods using alkyl chains of different length. For this purpose a mesoporous silica structure was constructed, taking as base the plane (1-11) of the β -cristoballite structure on which

large hexagonal nanopores were included, in order to simulate the mesoporous local surface structure. The calculations were carried out on a hexagonal unit cell that contains pores and wall thickness similar to those found in solids of the MCM-41 family. On this scaffold, alkyl chains of different lengths were anchored to the external surface. Due to the huge size of the models needed for this kind of study, the calculations were carried out using force field methods. Moreover, in order to find the global energy minimum and because of the presence of many local minima, molecular dynamics simulations were done to cover the more important parts of the potential energy surface using the thermal energy to go out of the local minima. These molecular dynamics simulations were carried out within the canonical ensemble (number of particles, volume and temperature were maintained constant) for a time of 10 ps with a time step of 1 fs at 298, 600 and 900K (these latter two high temperatures are used to quicker achieve a steady state thanks to chains faster motions).

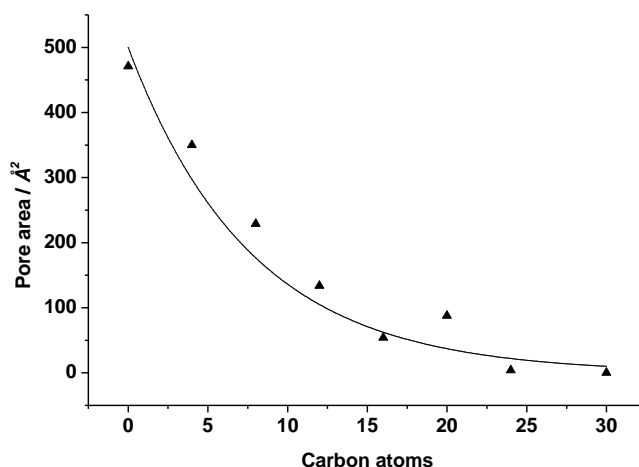


Figure 7. Dependence of the nanopore size (area in \AA^2) with the number of carbon atoms in the results of dynamic simulations achieved at 900 K. The line represents the best fit to an exponential law.

In the built models, the entrance of the nanopores did not show a regular shape. Thus, nanopore size after the molecular dynamics simulations was evaluated from the diameter of the biggest sphere able to move freely into and out of the nanopore or from the pore total surface when it is observed from the top. In both cases similar results were obtained. Figure 7 shows the dependence of the nanopore size with the

length of the n-alkyl groups resulting for the dynamic simulations at 900 K. Figure 8 shows perspective views of the surface models for alkyl chains containing 8, 12 and 16 carbon atoms.

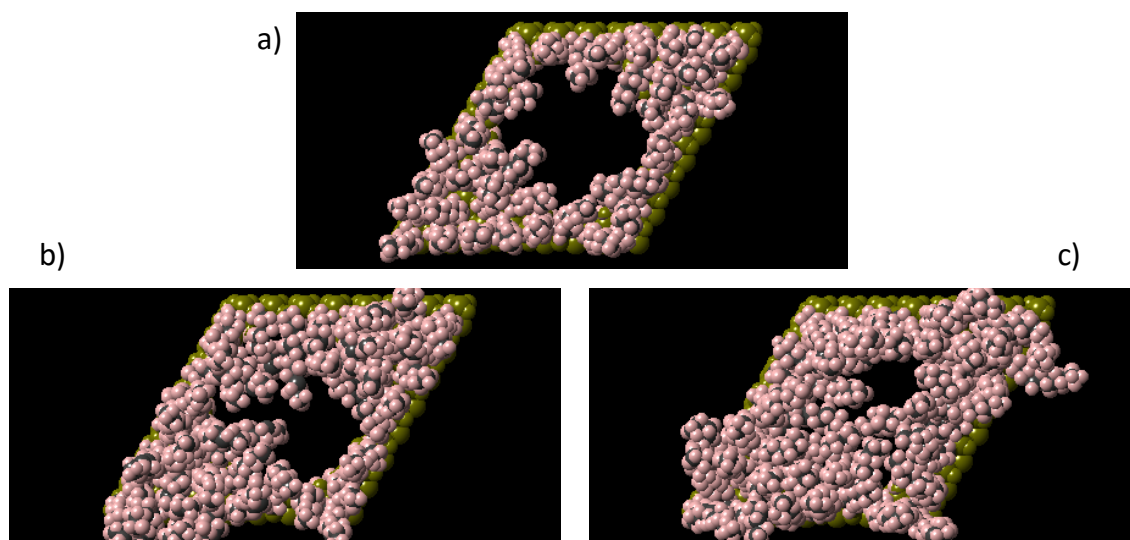


Figure 8. Perpendicular to the surface perspective views of obtained models for alkyl chains containing a) 8 b) 12 and c) 16 carbon atoms, at 900K. Pale yellow, grey and pink have been employed for mesoporous base, carbon and hydrogen atoms, respectively.

As it can be observed molecular dynamics predict in general a pore size reduction as the n-alkyl groups used in the built model became larger which in agreement with the experimental observation in relation to the rate of delivery for different solids. From the built models it was apparent that short n-alkyl chains were not large enough to fully/partially close the nanopore. In the case of longer chains, in the course of the dynamic simulations, it was found that alkyl groups displayed a high mobility due mainly to the lack of strong interactions between chains and they tend to freely and randomly move on the pore entrance only having occasional weak interactions with the neighboring chains. Therefore the built models showed that the pore was in a continuous opening/closure process. In fact in molecular dynamic studies at lower temperatures (298 and 600 K) it was found that the final nanopore size was strongly dependent on the starting conformation of the n-alkyl groups and on the simulation time. In fact data of pore sizes obtained at 298 and 600 K were in general worse than those obtained at 900 K. An

example of dynamic simulation displaying this effect of large mobility of the chains and continuous opening/closure process can be seen in a Quicktime video available in the Supporting Information (Animation from a molecular dynamic at 298 K that was 20 ps long (time step equal to 1 fs) on the mesoporous model with C16 groups anchored in its surface).

Since short n-alkyl chains are not large enough to fully/partially close the nanopore, it is clear that they cannot avoid the release of the ruthenium complex. Nevertheless, it could be expected that larger n-alkyl groups could close the pore due to its size, and they partially do, but not in a rigid fashion because the mentioned continuous opening/closure process related with the weak interactions between them. Therefore, although an experimental decrease of the release of ruthenium complexes was observed for large alkyl chains, dye massive leak can be expected for all systems from molecular modeling calculations. The poor interaction between alkyl chains in these systems and their effect on the nanopore size become more apparent if we compare, for a similar molecular length, the behavior of anchored alkyl chains and anchored protonated polyamines that are expected to strongly interact via repulsion electrostatic forces. For instance Figure 9 shows a parallel perspective views of the surfaces of geometry optimized models of anchored alkyl chain containing 16 carbon atoms and the anchoring of the parent triamine $[-C_4H_8NH_2C_3H_6NH_2C_3H_6NH_2C_3H_7]^{3+}$. Note that although molecular dynamics studies for the alkyl chain containing 16 carbon atoms lead at 900K to a partial pore closure (see Figure 8), the simple geometry optimization of the anchored chain resulted to a poor pore coverage (see Figure 9) in clear contrast to what was observed for the parent triamine which became rigid due to strong repulsive interactions between positively charged ammonium groups thus leading to a more effective pore closure (see Figure 9). Thus, for a similar chain size, protonated polyamines are able to induce a more effective pore closure than the corresponding alkyl chain. This is in agreement with previously reported results in amine-functionalized mesoporous materials.

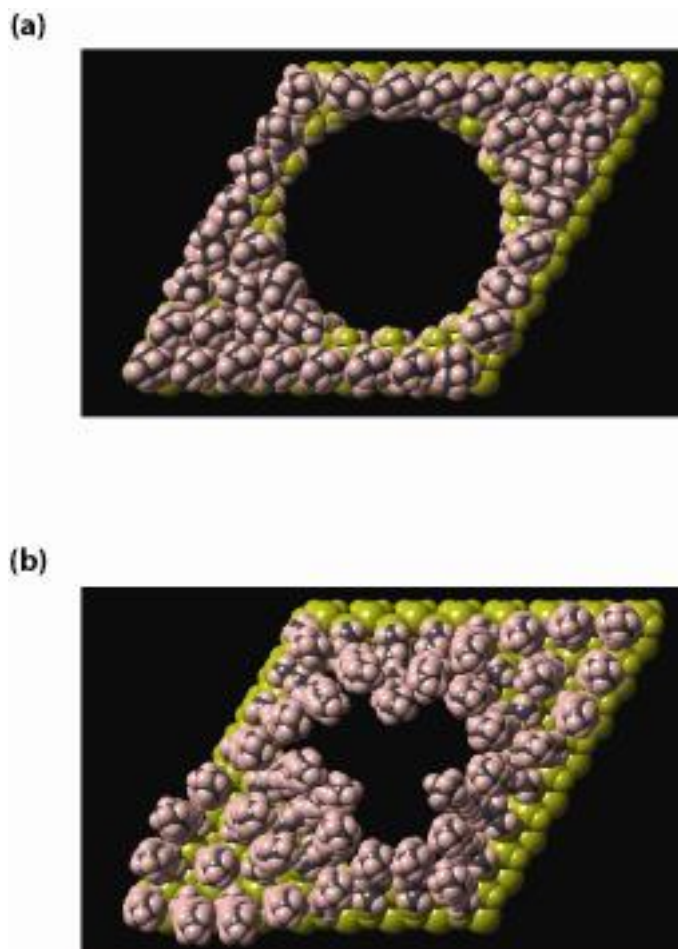


Figure 9. Perpendicular to the surface perspective views of geometry optimized models with hexadecyl groups (a) and its similar protonated triamine $[-C_4H_8NH_2C_3H_6NH_2C_3H_6NH_2C_3H_7]^{3+}$ (b). Pale yellow, blue, grey and pink have been employed for mesoporous base, nitrogen, carbon and hydrogen atoms, respectively.

CONCLUSIONS

The study of new protocols for controlled release is a captivating area for scientists due to its possible impact in the development of new technologies for cargo delivery applications. We have reported herein that mass delivery can be regulated by anchoring alkyl chains on the pore outlets of a silica mesoporous support. The release rate of the entrapped dye is close dependent of the alkyl chain length anchored on the external surface of the mesoporous scaffolding. The tethered chains build a flexible obstacle that

although can have a remarkable effect in the release rate, are not capable of preventing the diffusion process from the pore voids. Delivery studies showed that the time necessary for delivery 50% of the dye ($t_{1/2}$) increases exponentially as a function of the number of carbon atoms in the alkyl chain. Moreover, differences observed in the dye release rate from different solids can be discussed in terms of a simple diffusion process following a Higuchi model. Molecular dynamics simulations using force field methods have been carried out to explain the experimentally observed behavior. For this purpose, a mesoporous silica structure was constructed taking as base the (1-11) plane of the β -cristoballite structure on which large hexagonal nanopores and anchored polyamines were included. From these calculations, molecular dynamics predicted a pore size reduction as the n-alkyl groups used in the built model became larger. From the built models it was apparent that neither short nor long n-alkyl chains were able to fully close the nanopores. In all simulations weak interactions between the alkyl chains were found that led them to behave as loose threads. The obtained results may be of importance in the design of more sophisticated systems in which cargo payload rate may be important to control.

EXPERIMENTAL SECTION

Synthesis. General methods. XRD, TG analysis, elemental analysis, EDX microscopy, N₂ adsorption-desorption, UV-visible spectroscopy, NMR and particle size analysis techniques were employed to characterize the materials obtained. X-ray measurements were performed on a Bruker AXS D8 Advance using Cu-K α radiation. Thermo-gravimetric analyses were carried out on a TGA/SDTA 851e Mettler Toledo balance, using an oxidant atmosphere (Air, 80 mL/min) with a heating program consisting of a dynamic segment (10 °C per minute) from 298 K to 1273 K followed by a 1273 K isothermal segment for 30 min. EDX analyses were performed on a Jeol JSM 6300 operated at 20kV. TEM images were obtained with a 100kV Philips CM10 microscope. N₂ adsorption-desorption isotherms were recorded on a Micromeritics ASAP2010 automated sorption analyzer. The samples were degassed at 120 °C in vacuum overnight. The specific surface areas were calculated from the adsorption data in the low

pressures range using the BET model. Pore size was determined following the BJH method. UV-visible spectroscopy was carried out with a Lambda 35 UV/Vis Spectrometer (Perkin Elmer Instruments).

The reagents employed in the synthesis of solid **C0**, tetraethyl orthosilicate (TEOS), n-cetyltrimethylammonium bromide (CTABr), and triethanolamine (TEAH₃) were purchased from Fluka. Sodium hydroxide (NaOH) and acetonitrile were purchased from Scharlau. The dye [Ru(bipy)₃]Cl₂ was provided by Aldrich. The reagents ethyltrimethoxysilane for **C2**, butyltrimethoxysilane for **C4**, hexyltrimethoxysilane for **C6**, octyltriethoxysilane for **C8**, decyltriethoxysilane for **C10**, octadecyltrimethoxysilane for **C18**, docosyltrichlorosilane for **C22** and triacontyltrichlorosilane for **C30** employed in the synthesis of solids, were purchased from ABCR and anhydrous toluene was purchased from Scharlau. All the reactives were used as received without further purification.

Synthesis of MCM-41. The MCM-41 mesoporous nanoparticles were synthesized by the following procedure: n-cetyltrimethylammoniumbromide (CTABr, 1.00 g, 2.74 mmol) was first dissolved in 480 mL of deionized water. Then, 3.5 mL of a NaOH 2.00 mol L⁻¹ solution was added followed by an adjustment of the temperature to 80 °C. TEOS (5.00 mL, 22.4 mmol) was then added dropwise to the surfactant solution. The mixture was stirred for 2 hours to give a white precipitate. Finally the solid was collected by centrifugation, washed with deionized water and dried at 70 °C overnight (MCM-41 as-synthesized). To prepare the final porous material (MCM-41), the as-synthesized solid was calcined at 550 °C using an oxidant atmosphere for 5 hours in order to remove the template phase.

Synthesis of C0. In a typical synthesis, 1 g of the MCM-41 solid were suspended in 40 ml of anhydrous acetonitrile and heated in a Dean-Stark in order to remove the adsorbed water in the mesoporous support. Then tris(2,2'-bipyridyl)ruthenium(II) chloride dye (0.6 g, 0.8 mmol) was added to the suspension and stirred for 24 hours at room temperature with the aim of loading the pores of the MCM-41 scaffolding. After this loading procedure, the orange solid (**C0**) was filtered, washed with acetonitrile and dried at 50 °C for 12 h.

Synthesis of solids C2, C4, C6, C8, C10 and C18. In a typical synthesis, 0.15 g of the **C0** solid were suspended in 4.5 ml of anhydrous toluene and 3 mmol of the corresponding silane

(ethyltrimethoxysilane for **C2**, butyltrimethoxysilane for **C4**, hexyltrimethoxysilane for **C6**, octyltriethoxysilane for **C8**, decyltriethoxysilane for **C10** and octadecyltrimethoxysilane for **C18**) was added to the suspension and stirred vigorously for 5.5 hours. The resulting orange solid was filtered, washed with toluene and dried at 50 °C for 12 h. This synthetic procedure assures a preferential grafting of the alkyl chain in the pore outlets rather than inside the pore walls, which are basically filled by the ruthenium (II) dye.

Synthesis of solid C22. In a typical synthesis, 0.15 g of the **C0** solid were suspended in 4.5 ml of anhydrous toluene and 2 mmol of docosyltrichlorosilane was added to the suspension and stirred vigorously for 10 minutes. The resulting orange solid was filtered, washed with toluene and dried at 50 °C for 12 h. This synthetic procedure assures a preferential grafting of the alkyl chain in the pore outlets rather than inside the pore walls, which are basically filled by the ruthenium (II) dye.

Synthesis of solid C30. In a typical synthesis, 0.15 g of the **C0** solid were suspended in 4.5 ml of anhydrous toluene at 60 °C and 2 mmol of triacontyltrichlorosilane were added to the suspension under vigorous stirring for 10 minutes. The resulting orange solid was filtered, washed with toluene and dried at 50 °C for 12 h. This synthetic procedure assures a preferential grafting of the alkyl chain in the pore outlets rather than inside the pore walls, which are basically filled by the ruthenium (II) dye.

Dye release studies. In a typical synthesis, 2 mg of the corresponding solid and 10 mL of deionized water were maintained under constant vigorous stirring for a certain time and then, the suspension was filtered off through a 0.45 µm nylon filter. The delivery of the ruthenium(II) dye from the pore voids to the aqueous solution was monitored via the band of the dye centered at 454 nm.

Computational Details. Just like in previous works, the two-dimensional model of a mesoporous silica of the MCM-41 family was built from the crystal structure of β -cristoballite. A cleavage of the crystal structure parallel to the (1-11) plane allowed us to obtain a mesoporous model with large quasi-cylindrical nanopores. This model can be described as a hexagonal supercell with the following parameters, $a = b = 40.503 \text{ \AA}$, $\alpha = \beta = 90.0^\circ$ and $\gamma = 120.0^\circ$. The size of this “supercell” was chosen in order to generate pores and walls with similar dimensions (diameter, $d = 22.9 \text{ \AA}$ and thickness, $t = 15.5$

Å, respectively) to those experimentally found in MCM-41 family solids ($d = 23.3$ Å and $t = 13.1$ Å). The deepness of the pores in this two-dimensional model is 28.7 Å. The terminal oxygen atoms in the surfaces and inside the nanopore were protonated. In our system, alkyl groups were anchored in the surface. This process was done with Material Studio package,³⁵ Experimental data suggest that all possible anchoring points must be used. So, to avoid problems caused by steric effects between neighboring receivers, lineal alkyl fragments were firstly anchored and then a relaxation of their geometries was allowed. In this model, the size of the alkyl chain anchored in the surface did stretch from 4 to 30, where this number alludes to the number of carbon atoms in the group.

Due to the huge size of the models needed for this kind of study, the calculations were carried out using force field methods. For this purpose, the universal force field (UFF) suggested by Rappe et al. was employed.³⁶ In order to find the global energy minimum and because of the presence of many local minima, molecular dynamics simulations were done to cover the more important parts of the potential energy surface using the thermal energy to go out of the local minima. These molecular dynamics simulations were carried out within the canonical ensemble (number of particles, volume and temperature were maintained constant) for a time of 10 ps with a time step of 1 fs at 298, 600 and 900K. Among the conformations observed during the molecular dynamics simulation, the most stable geometry was taken as starting point for a later geometry optimization. The geometry optimizations and molecular dynamics simulations were performed with the Material Studio package. In the evaluation of the nanopore area (Figure 7), the Van der Waals radii provided by the Material Studio package for each element were used. The nanopore diameter has been evaluated that represents the maximum diameter of a sphere that moves freely into and out of nanopore.

ACKNOWLEDGMENT. Financial support from the Spanish Government (project MAT2009-14564-C04-01 and MAT2009-14564-C04-04), the Generalitat Valencia (project PROMETEO/2009/016) is gratefully acknowledged.

-
- ¹ Hamidi, M.; Azadi, A.; Rafiei, P. *Adv. Drug Delivery Rev.* **2008**, *60*, 1638 – 1649.
- ² Pouton, C.W.; Porter, C.J.H. *Adv. Drug Delivery Rev.* **2008**, *60*, 625 – 637.
- ³ Rijcken, C.J.F.; Soga, O.; Hennink, W.E.; van Nostrum, C.F. *J. Controlled Release* **2007**, *120*, 131 – 148.
- ⁴ Boas, U.; Heegaard, P.M.H. *Chem. Rev.* **2004**, *33*, 43-63.
- ⁵ Uhrich, K.E.; Cannizzaro, S.M.; Langer, R.S; Shakesheff, K.M. *Chem. Rev.* **1999**, *99*, 3181-3198.
- ⁶ (a) Kresge, C.T.; Leonowicz, M.E.; Roth, W.J.; Vartuli, J.C.; Beck, J.S. *Nature*, **1992**, *359*, 710-712. (b) Zhao, D.; Feng, J.; Huo, Q.; Melosh, N.; Fredrickson, G.H.; Chmelka, B.F.; Stucky, G.D. *Science*, **1998**, *279*, 548-552. (c) Liu, Y.; Zhang, W.; Pinnavaia, T.J. *Angew. Chem. Int. Ed.* **2001**, *40*, 1255-1258. (d) Han, Y.; Li, D.; Zhao, L.; Xiao, F.-S. *Angew. Chem. Int. Ed.* **2003**, *42*, 3633-3638. (e) Beck, J.S.; Vartuli, J.C.; Roth, W. J.; Leonowicz, M.E.; Kresge, C.T.; Schmitt, K.D.; Chu, C.T.-W; Olson, D.H.; Sheppard, E.W.; McCullen, S.B.; Higgins, J.B.; Schlenker, J.L. *J. Am. Chem. Soc.* **1992**, *114*, 10834-10843. (f) A.P. Wright, M. E. Davis, *Chem. Rev.* **2002**, *102*, 3589-3614. (c) G. Kickelbick, *Angew. Chem.* **2004**, *116*, 3164-3166; *Angew. Chem. Int. Ed.* **2004**, *43*, 3102-3104.
- ⁷ Vallet-Regí, M.; Rámila, A.; del Real, R.P.; Pérez-Pariente, J. *J. Chem. Mater.* **2001**, *13*, 308–311.
- ⁸ (a) Muñoz, B.; Rámila, A.; Pérez-Pariente, J.; Díaz, I.; Vallet-Regí, M. *Chem. Mater.* **2003**, *15*, 500–503. (b) Vallet-Regí, M.; Balas, F.; Arcos, D. *Angew.Chem. Int. Ed.* **2007**, *46*, 7548–7558.
- ⁹ (a) Trewyn, B. G.; Slowing, I. I.; Giri, S.; Chen, H.-T.; Lin, V.S.-Y. *Acc. Chem. Res.* **2007**, *40*, 846–853. (b) Slowing, I.I.; Vivero-Escoto, J.L.; Wu, C.W.; Lin, V.S.-Y *Adv. Drug Deliv. Rev.* **2008**, *60*, 1278-1288. (c) Aznar, E.; Martínez-Máñez, R.; Sancenón, F. *Expert Opin. Drug Deliv.* **2009**, *6*, 643-655. (d) Cotí, K.; Belowich, M. E.; Liong, M.; Ambrogio, M.W.; Lau, Y.A.; Khatib, H.A.; Zink, J.I.; Khashab, N.M.; Stoddart, J.F. *Nanoscale*, **2009**, *1*, 16-39.

¹⁰ (a) Mal, N. K.; Fujiwara, M.; Tanaka, Y. *Nature* **2003**, *421*, 350–353. (b) Mal, N. K.; Fujiwara, M.; Tanaka, Y.; Taguchi, T.; Matsukata, M. *Chem. Mater.* **2003**, *15*, 3385–3394.

¹¹ (a) Zhu, Y.; Fujiwara, M. *Angew. Chem. Int. Ed.* **2007**, *46*, 2241–2244. (b) Lu, J.; Choi, E.; Tamanoi, F.; Zink, J. I. *Small* **2008**, *4*, 421–426. (c) Angelos, S.; Vhoi, E.; Vögtle, F.; De Cola, L.; Zink, J. I. *J. Phys. Chem. C* **2007**, *111*, 6589–6592. (d) Liu, N. G.; Chen, Z.; Dunphy, D. R.; Jiang, Y. –B.; Assink, R. A.; Brinker, C. J. *Angew. Chem. Int. Ed.* **2003**, *42*, 1731–1734.

¹² (a) Liu, N.; Dunphy, D.; Atanassov, P.; Bunge, S. D.; Chen, Z.; López, G. P.; Boyle, T. J.; Brinker, C. J. *Nano Lett.* **2004**, *4*, 551–554. (b) Ferris, D. P.; Zhao, Y.-L.; Khashab, N. M.; Khatib, H. A.; Stoddart, J. F.; Zink, J. I. *J. Am. Chem. Soc.* **2009**, *131*, 1686–1688. (c) Park, C.; Lee, K.; Kim, C. *Angew. Chem., Int. Ed.* **2009**, *48*, 1275–1278.

¹³ Aznar, E.; Casasús, R.; García-Acosta, B.; Marcos, M. D.; Martínez-Máñez, R.; Sancenón, F.; Soto, J.; Amorós, P. *Adv. Mater.* **2007**, *19*, 2228–2231.

¹⁴ (a) Casasús, R.; Marcos, M. D.; Martínez-Máñez, R.; Ros-Lis, J. V.; Soto, J.; Villaescusa, L. A.; Amorós, P.; Beltrán, D.; Guillem, C.; Latorre, J. *J. Am. Chem. Soc.* **2004**, *126*, 8612–8613. (b) Casasús, R.; Climent, E.; Marcos, M. D.; Martínez-Máñez, R.; Sancenón, F.; Soto, J.; Amorós, P.; Cano, J.; Ruiz, E. *J. Am. Chem. Soc.* **2008**, *130*, 1903–1917. (c) Bernardos, A.; Aznar, E.; Coll, C.; Martínez-Máñez, R.; Barat, J. M.; Marcos, M. D.; Sancenón, F.; Soto, J. *J. Controlled Release* **2008**, *131*, 181–189.

¹⁵ Yang, Q.; Wang, S.; Fan, P.; Wang, L.; Di, Y.; Lin, K.; Xiao, F.-S. *Chem. Mater.* **2005**, *17*, 5999–6003.

¹⁶ (a) Nguyen, T. D.; Leung, K.C.-F.; Liong, M.; Pentecost, C. D.; Stoddart, J. F.; Zink, J. I. *Org. Lett.* **2006**, *8*, 3363–3366. (b) Leung, K.C.-F.; Nguyen, T. D.; Stoddart, J. F.; Zink, J. I. *Chem. Mater.* **2006**, *18*, 5919–5928. (c) Park, C.; Oh, K.; Lee, S. C.; Kim, C. *Angew. Chem., Int. Ed.* **2007**, *46*, 1455–1457.

(d) Angelos, S.; Yang, Y.-W.; Khashab, N. M.; Stoddart, J. F.; Zink, J. I. *J. Am. Chem. Soc.* **2009**, *131*, 11344–11346.

¹⁷ (a) Angelos, S.; Yang, Y.-W.; Patel, K.; Stoddart, J. F.; Zink, J. I. *Angew. Chem., Int. Ed.* **2008**, *47*, 2222–2226. (b) Khashab, N. M.; Belowich, M. E.; Trabolsi, A.; Friedman, D. C.; Valente, C.; Lau, Y.; Khatib, H. A.; Zink, J. I.; Stoddart, J. F. *Chem. Commun.* **2009**, 5371–5373. (c) Angelos, S.; Khashab, N. M.; Yang, Y.-W.; Trabolsi, A.; Khatib, H. A.; Stoddart, J. F.; Zink, J. I. *J. Am. Chem. Soc.* **2009**, *131*, 12912–12914.

¹⁸ Khashab, N. M.; Trabolsi, A.; Lau, Y. A.; Ambrogio, M. W.; Friedman, D. C.; Khatib, H. A.; Zink, J. I.; Stoddart, J. F. *Eur. J. Org. Chem.* **2009**, 1669–1673.

¹⁹ Du, L.; Liao, S.; Khatib, H. A.; Stoddart, J. F.; Zink, J. I. *J. Am. Chem. Soc.* **2009**, *131*, 15136–15142.

²⁰ See as example: (a) Aznar, E.; Marcos, M. D.; Martínez-Máñez, R.; Sancenón, F.; Soto, J.; Amorós, P.; Guillem, C. *J. Am. Chem. Soc.* **2009**, *131*, 6833–6843. (b) Knežević, N.; Trewyn, B.G.; Lin, V.-Y. *Chem. Eur. J.* **2011**, *17*, 3338–3342.

²¹ (a) Trewyn, B. G.; Giri, S.; Slowing, I. I.; Lin, V.S.-Y. *Chem. Commun.* **2007**, 3236–3245. (b) Lai, C.-Y.; Trewyn, B. G.; Jeftinija, D. M.; Jeftinija, K.; Xu, S.; Jeftinija, S.; Lin, V.S.-Y. *J. Am. Chem. Soc.* **2003**, *125*, 4451–4459. (c) Torney, F.; Trewyn, B. G.; Lin, V.S.-Y.; Wang, K. *Nat. Nanotechnol.* **2007**, *2*, 295–300. (d) Radu, D. R.; Lai, C.-Y.; Jeftinija, K.; Rowe, E. W.; Jeftinija, S.; Lin, V.S.-Y. *J. Am. Chem. Soc.* **2004**, *126*, 13216–13217. (e) Giri, S.; Trewyn, B. G.; Stellmaker, M. P.; Lin, V.S.-Y. *Angew. Chem., Int. Ed.* **2005**, *44*, 5038–5044. (f) Slowing, I. I.; Trewyn, B. G.; Lin, V. S. -Y. *J. Am. Chem. Soc.* **2007**, *129*, 8845–8849. (g) Slowing, I. I.; Trewyn, B. G.; Giri, S.; Lin, V.S.-Y. *Adv. Funct. Mater.* **2007**, *17*, 1225–1236. (h) Vivero-Escoto, J. L.; Slowing, I. I.; Wu, C.-Y.; Lin, V.S.-Y. *J. Am. Chem. Soc.* **2009**, *131*, 3462–3463. (i) Mortera, R.; Vivero-Escoto, J.; Slowing, I. I.; Garrone, E.; Onida,

B.; Lin, V.S.-Y. *Chem. Commun.* **2009**, 321–3221. (j) Zhao, Y.; Trewyn, B. G.; Slowing, I. I.; Lin, V.S.-Y. *J. Am. Chem. Soc.* **2009**, *131*, 8398–8400.

²² (a) Hernandez, R.; Tseng, H.-R.; Wong, J. W.; Stoddart, J. F.; Zink, J. I. *J. Am. Chem. Soc.* **2004**, *126*, 3370–3371. (b) Nguyen, T. D.; Tseng, H.-R.; Celeste, P. C.; Flood, A. H.; Liu, Y.; Stoddart, J. F.; Zink, J. I. *Proc. Natl. Acad. Sci., U.S.A.* **2005**, *102*, 10029–10034. (c) Nguyen, T. D.; Liu, Y.; Saha, S.; Leung, K.C.-F.; Stoddart, J. F.; Zink, J. I. *J. Am. Chem. Soc.* **2007**, *129*, 626–634. (d) Nguyen, T. D.; Leung, K.C.-F.; Liong, M.; Liu, Y.; Stoddart, J. F.; Zink, J. I. *Adv. Funct. Mater.* **2007**, *17*, 2101–2110. (e) Angelos, S.; Liong, M.; Choi, E.; Zink, J. I. *Chem. Eng. J.* **2008**, *137*, 4–13.

²³ (a) Fujiwara, M.; Terashima, S.; Endo, Y.; Shiokawa, K.; Ohue, H. *Chem. Commun.* **2006**, 4635–4637. (b) Liu, R.; Zhao, X.; Wu, T.; Feng, P. *J. Am. Chem. Soc.* **2008**, *130*, 14418–14419. (c) Liu, R.; Zhang, Y.; Feng, P. *J. Am. Chem. Soc.* **2009**, *131*, 15128–15129. (d) Porta, F.; Lamers, G.E.M.; Zink, J.I.; Kros, A. *J. Phys. Chem. C* **2011**, *13*, 9982–9985. (e) Luo, Z.; Cai, K.; Hu, Y.; Zhao, L.; Liu, P.; Duan, L.; Yang, W. *Angew. Chem., Int. Ed.* **2011**, *50*, 640–643.

²⁴ (a) Wan, X.; Zhang, G.; Liu, S. *Macromol. Rapid. Commun.* **2011**, *32*, 1082–1089. (b) Liu, R.; Liao, P.; Liu, J.; Feng, P. *Langmuir* **2011**, *27*, 3095–3099. (c) Xue, M.; Zhong, X.; Sahposhnik, Z.; Qu, Y.; Tamanoi, F.; Duan, X.; Zink, J.I. *J. Am. Chem. Soc.* **2011**, *133*, 8798–8801. (d) Muhammad, F.; Guo, M.; Qi, W.; Sun, F.; Wang, A.; Guo, Y.; Zhu, G. *J. Am. Chem. Soc.* **2011**, *133*, 8778–8781. (e) Zhang, F.; Clime, L.; Roberge, H.; Normandin, F.; Yahia, L'H.; Sacher, E.; Veres, T. *J. Phys. Chem. C* **2011**, *115*, 1436–1443. (f) Zheng, H.; Gao, C.; Peng, B.; Shu, M.; Che, S. *J. Phys. Chem. C* **2011**, *115*, 7230–7237. (g) Yuan, L.; Tang, Q.; Yang, D.; Zhang, J.Z.; Zhang, F.; Hu, J. *J. Phys. Chem. C* **2011**, *115*, 9926–9932. (h) Schlossbauer, A.; Dohmen, C.; Schaffert, D.; Wagner, E.; Bein, T. *Angew. Chem., Int. Ed.* **2011**, *50*, 6828–6930. (i) Zhou, K.; Wang, Y.; Huang, X.; Luby-Phelps, K.; Sumer, B.D.; Gao, J. *Angew. Chem., Int. Ed.* **2011**, *50*, 6109–6114.

²⁵ (a) Fu, Q.; Rao, G. V. R.; Ista, L. K.; Wu, Y.; Andrzejewski, B. P.; Sklar, L. A.; Ward, T. L.; López, G. P. *Adv. Mater.* **2003**, *15*, 1262–1266. (b) Fu, Q.; Rao, G. V. R.; Ward, T.L.; Lu, Y.; López, G. P. *Langmuir* **2007**, *23*, 170–174. (c) Zhou, Z.Y.; Zhu, S.M.; Zhang, D. *J. Mater. Chem.* **2007**, *17*, 2428–2433. (d) Zhu, S.; Zhou, Z.; Zang, D.; Jin, C.; Li, Z. *Micropor. Mesopor. Mater.* **2007**, *106*, 56–61. (e) Zhu, Y.; Kaskel, S.; Ikoma, T.; Haganata, N. *Micropor. Mesopor. Mater.* **2009**, *123*, 107–112. (f) You, Y.-Z.; Kalebaila, K.K.; Brock, S.L.; Oupicky, D. *Chem. Mater.* **2008**, *20*, 3354–3359. (g) Liu, C; Guo, J; Yang, W; Hu; J, Wang, C; Fu, S; *J. Mater. Chem.* **2009**, *19*, 4764–4770. (h) Schossbauer, A.; Warncke, S.; Gramlich, P. M. E.; Kecht, J.; Manetto, A.; Carell, T.; Bein, T. *Angew. Chem. Int. Ed.*, **2010**, *49*, 4734–4737. (i) Aznar, E.; Mondragón, L.; Ros-Lis, J.V.; Sancenón, F.; Marcos, M. D.; Martínez-Máñez, R.; Soto, J.; Pérez-Payá, E.; Amorós, P. *Angew. Chem., Int. Ed.* **2011**, doi 10.1002/ange.201102756.

²⁶ Coll, C.; Casasús, R.; Aznar, E.; Marcos, M. D.; Martínez-Máñez, R.; Sancenón, F.; Soto, J.; Amorós, P. *Chem. Commun.* **2007**, 1957–1959. (b) Casasús, R.; Aznar, E.; Marcos, M. D.; Martínez-Máñez, R.; Sancenón, F.; Soto, J.; Amorós, P. *Angew. Chem., Int. Ed.* **2006**, *45*, 6661–6664. (c) Aznar, E.; Coll, C.; Marcos, M. D.; Martínez-Máñez, R.; Sancenón, F.; Soto, J.; Amorós, P.; Cano, J.; Ruíz, E. *Chem.-Eur. J.* **2009**, *15*, 6877–6888. (d) Climent, E.; Marcos, M. D.; Martínez-Máñez, R.; Sancenón, F.; Soto, J.; Rurack, K.; Amorós, P. *Angew. Chem., Int. Ed.* **2009**, *48*, 8519–8522. (e) Coll, C.; Aznar, E.; Martínez-Máñez, R.; Marcos, M. D.; Sancenón, F.; Soto, J.; Amorós, P.; Cano, J.; Ruíz, E. *Chem.-Eur. J.* **2010**, *16*, 10048–10061. (f) Candel, I.; Bernardos, A.; Climent, E.; Marcos, M. D.; Martínez-Máñez, R.; Sancenón, F.; Soto, J.; Costero, A.; Gil, S.; Parra, M. *Chem. Commun.* **2011**, *47*, 8313–8315. (g) Lee, J., Lee, J.; Kim, S.; Kim, C.-j.; Lee, S.; Min, B.; Shin, Y.; Kim, C. *Bull. Korean Chem. Soc.* **2011**, *32*, 1357–1360.

²⁷ (a) Patel, K.; Angelos, S.; Dichtel, W. R.; Coskun, A.; Yang, Y.-W.; Zink, J. I.; Stoddart, J. F. *J. Am. Chem. Soc.* **2008**, *130*, 2382–2383. (b) Klichko, Y.; Khashab, N. -M.; Yang, Y. -W.; Angelos, S.; Stoddart, J. F.; Zink, J. I. *Microporous Mesoporous Mater.* **2010**, *132*, 435–441. (c) Schlossbauer, A.;

Kecht, J.; Bein, T. *Angew. Chem., Int. Ed.* **2009**, *48*, 3092–3095. (d) Bernardos, A.; Aznar, E.; Marcos, M. D.; Martínez-Máñez, R.; Sancenón, F.; Soto, J.; Barat, J. M.; Amorós, P. *Angew. Chem., Int. Ed.* **2009**, *48*, 5884–5887. (e) Park, C.; Kim, H.; Kim, S.; Kim, C. *J. Am. Chem. Soc.* **2009**, *131*, 16614–16615. (f) Bernardos, A.; Mondragón, L.; Aznar, E.; Marcos, M. D.; Martínez-Máñez, R.; Sancenón, F.; Soto, J.; Barat, J. M.; Pérez-Payá, E.; Guillem, C.; Amorós, P. *ACSNano* **2010**, *4*, 6353–6368. (g) Coll, C.; Mondragón, L.; Martínez-Máñez, R.; Sancenón, F.; Marcos, M. D.; Soto, J.; Amorós, P.; Pérez-Payá, E. *Angew. Chem., Int. Ed.* **2011**, *50*, 2138–2140. (h) Liu, J.; Du, X.; Zhang, X. *Chem.-Eur. J.* **2011**, *17*, 810–815.

²⁸ Climent, E.; Bernardos, A.; Martínez-Máñez, R.; Maquieira, A.; Marcos, M. D.; Pastor-Navarro, N.; Puchades, R.; Sancenón, F.; Soto, J.; Amorós, P. *J. Am. Chem. Soc.* **2009**, *131*, 14075–14080.

²⁹ Zhu, C.-L.; Lu, C.-H.; Song, X.-Y.; Yang, H.-H.; Wang, X.-R. *J. Am. Chem. Soc.* **2011**, *133*, 1278–1281.

³⁰ Climent, E.; Martínez-Máñez, R.; Sancenón, F.; Marcos, M. D.; Soto, J.; Maquieira, A.; Amorós, P. *Angew. Chem., Int. Ed.* **2010**, *49*, 7281–7283.

³¹ (a) Hoffmann, F.; Cornelius, M.; Morell, M.; Fröba, M. *Angew. Chem. Int. Ed.* **2006**, *45*, 3216–3251. (b) Descalzo, A.B.; Martínez-Máñez, R.; Sancenón, F.; Hoffmann, K.; Rurack, K. *Angew. Chem. Int. Ed.* **2006**, *45*, 5924–5948. (c) Ariga, K.; Vinu, A.; Hill, J.P.; Mori, T. *Coord. Chem. Rev.* **2007**, *251*, 2562 – 2591; d) Martínez-Máñez, R.; Sancenón, F. *Coord. Chem. Rev.* **2006**, *250*, 3081 –3093; e) Ariga, K.; Hill, J.P.; Lee, M.V.; Vinu, A.; Charvet, R.; Acharya, S. *Sci. Technol. Adv. Mater.* **2008**, *9*, 014109.

³² Gartmann, N.; Brühwiler, D. *Angew. Chem. Int. Ed.* **2009**, *48*, 6354 –6356.

³³ Nakanishi, T.; Shen, Y.; Wang, J.; Li, H.; Fernandes, P.; Yoshida, K.; Yagai, S.; Takeuchi, M.; Ariga, K.; Kurth, D.G.; Möwald, H. *J. Mater. Chem.* **2010**, *20*, 1253–1260.

³⁴ (a) Higuchi, T. *J. Pharm. Sci.* **1961**, *50*, 874-875. (b) Higuchi, T. *J. Pharm. Sci.* **1963**, *52*, 1145-1149.

³⁵ *Material Studio*, version 4.1; Molecular Simulations Inc.: San Diego, CA, 1998.

³⁶ (a) Rappe, A.K.; Casewith, C.J.; Colwell, K.S.; Goddard-III, W.A.; Skiff, W.M. *J. Am. Chem. Soc.*, **1992**, *114*, 10024-10035. (b) Castonguay, L.A.; Rappe, A.K. *J. Am. Chem. Soc.*, **1992**, *114*, 5832-5842. (c) Rappe, A.K.; Colwell, K.S. *Inorg. Chem.*, **1993**, *32*, 3438-3450.

FOR TABLE OF CONTENTS USE ONLY

Delivery modulation in silica mesoporous supports via alkyl chain pore outlet decoration.

Elena Aznar, Félix Sancenón, M. Dolores Marcos, Ramón Martínez-Mañez, Pieter Stroeve, Joan Cano and Pedro Amorós.

